NOTES AND CORRESPONDENCE

Simulation of the Orographic Influence on Weather Radar Using a Geometric–Optics Approach

M. GABELLA AND G. PERONA

Dipartimento di Elettronica, Politecnico di Torino, Torino, Italy

18 February 1997 and 15 December 1997

ABSTRACT

A computer code for radar site assessment, including ground clutter, beam occultation, and earth curvature–atmospheric refraction factors, has been developed. The code uses topographic information in the form of a raster Digital Elevation Model, air refractive index profile in the boundary layer, surface backscattering cross section per unit area at grazing angles as derived from literature, and ancillary information, if available, derived from a land use–land cover map. This algorithm is independent of a specific radar site and radar system. Several benefits in dealing with open problems of radar meteorology and of radar design could be derived from its use, namely, better estimate of precipitation at ground level through vertical echo profile correction, scanning strategy, land clutter measurements at low grazing angles, and characterization of seasonal and topographic effects. The raster-based approach used in implementing the code makes it compatible with any spatial resolution desired. Simplicity and short simulation times have been pursued as primary goals during the planning and implementation phases of the code. The result is a standard ANSI FORTRAN software that is portable, easy to use, and runs on an IBM-compatible PC. In its simplest version, the model needs only a raster Digital Elevation Model, the radar parameters, and an estimate of the mean atmospheric refraction.

1. Introduction

A meteorological radar is a powerful sensor to estimate rainfall over large areas. However, the precipitation at ground level must be deduced from measurements aloft and, consequently, considerable errors may result since variations in the vertical reflectivity profile often occur. Even in flat regions, unexpectedly large errors may appear because of the reduced visibility due to earth curvature and refractive index effects; yet, the situation is especially severe in orographically complex regions. By comparing several years of radar–gauge data, Joss et al. (1995) and Joss and Lee (1995) have clearly shown the influence of the vertical echo structure, the width of the radar beam, and the topography around the radar upon the quality of precipitation estimate. The computer code described in this paper aims at contributing to the solution of the above items. In fact, it is able to characterize a priori the orographic environment for weather radars in terms of ground target and shielded areas. The ground clutter distribution estimate, for a given antenna radiation pattern and elevation angle, can be used for the preliminary characterization of a radar site (see, e.g., Smith 1972) and for the definition of suitable scanning strategies. Furthermore, the knowledge of the minimum height at which a volumetric pixel of the atmosphere may be seen by the radar beam above a shadowed area is in turn very useful in implementing correction procedures for the rainfall estimate associated to the vertical echo structure. The information obtained through the software tool presented here may be integrated within procedures using real-time radar-derived information (see, e.g., Joss and Lee 1995; Lee et al. 1995; Joss and Wessels 1990; Geotis and Silver 1976).

The structure of the software tool, (called Ground Echo Characterization Software GECS), is described in section 2, and a comparison between simulation results and experimental data relative to a radar located in Piemonte (northwest part of Italy) is presented in section 3.

2. GECS description

The GECS code flowchart is presented in Fig. 1. The software input is a raster Digital Elevation Model (DEM) map. Ray bending (block 1) is estimated through the use of the effective earth's radius model; for weather radar applications, this approach predicts beam height with sufficient accuracy as long as the refractive index profile gradient is constant throughout the first kilometer of the atmosphere (see, e.g., Doviak and Zrnic 1993). GECS uses a single equivalent earth's radius for all

Corresponding author address: Dr. Marco Gabella, Dipartimento di Elettronica, Politecnico di Torino, C.so Duca degli Abruzzi, 24, I-10129 Torino, Italy.
E-mail: gabella@phoen.polito.it

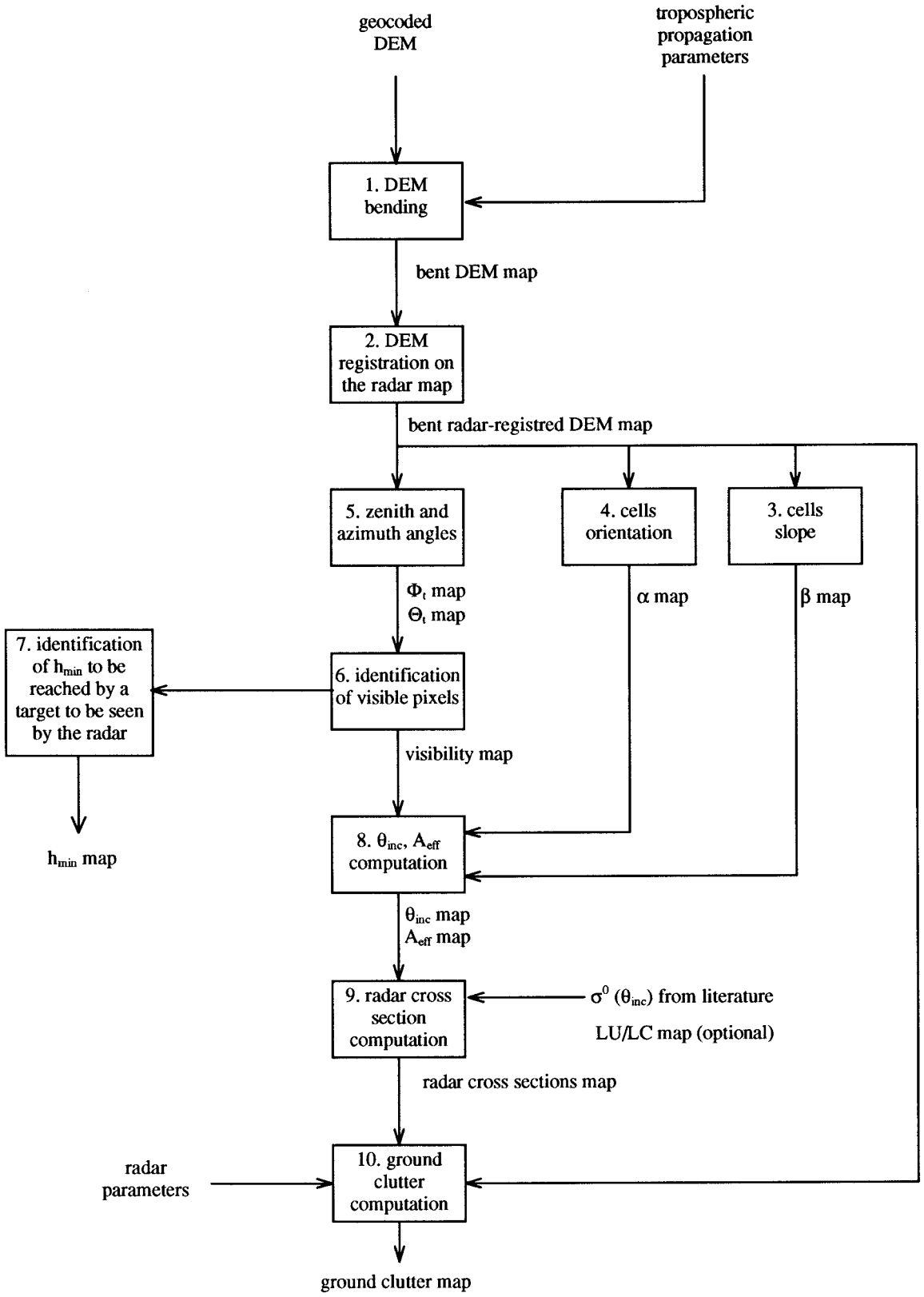

FIG. 1. Ground echo characterization software flowchart.

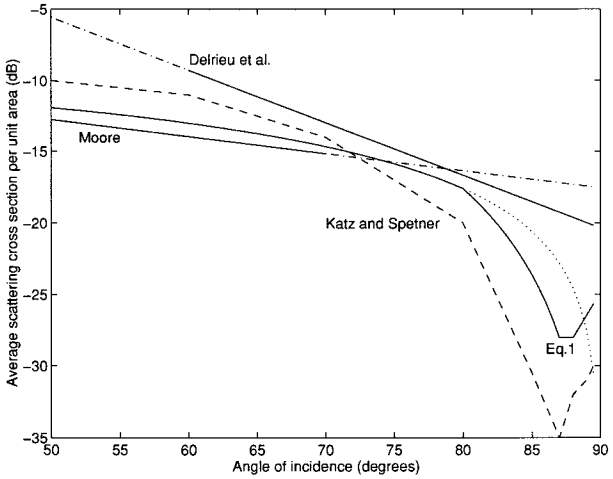

FIG. 2. Average scattering cross section per unit area, $\overline{\sigma}^0_{\mathrm{dB}}$, at large angles of incidence.

TABLE 1. The Regione Piemonte radar parameters.

Transmitter–receiver	
Peak power	158 kW
Frequency	5.7 GHz
PRF	259 Hz
Pulse duration	2 μs
MDS	−103 dBm
Antenna	
Diameter	2.4 m
Beamwidth at half power	1.54°
Power gain	40 dB
Polarization	Horizontal
Data features	
Maximum range used	240 km
Radial resolution	250 m × 4 m
Number of power levels	128

directions around the radar; this is adequate on average for the results presented in this paper. Should we wish to explain details on a given clutter pixel, we would need corresponding details on obstacles (DEM) and refractive index structure (ray tracing).

If high precision is needed, the bent DEM needs to be registered on the same geographic reference system of the meteorological radar data maps. In the present example, the Regione Piemonte radar data (see section 3) were projected on a reference plane tangential to the geoid at the radar site having the local meridian as a reference. Therefore, a registration and resampling routine has been developed to calculate the results on a Cartesian (x, y) radar grid map (block 2). Errors caused by this transformation remain below 40 m at 200 km range.

The implemented algorithms performing pixels slope (β) and orientation (α) assessment (blocks 3 and 4) give outputs that are consistent with the results of commercial tools [e.g., the SURFACE© routine within the IDRISI GIS software (Eastman 1990)].

A radar-target zenith angle (Φ_t) and an azimuth angle (Θ_t) are calculated (block 5) in a spherical reference system (from the center of the focus of the radar antenna to the center of each DEM pixel).

The above angles are then used for estimating the visibility of each pixel as seen by the radar antenna (block 6). The geometric optics approach has been used to characterize a pixel's visibility. Pixels can then be identified out of the shadow of obstacles closer to the radar. Of course, for a more precise estimate of shadowing effects, the diffraction theory should be used where the geometric optics theory predicts zero illumination (Doviak and Zrnic 1985); evidently, the procedure would be time consuming and eventually impossible because of the lack of details in the DEM and the refractive index structure. According to the geometric optics approach used, a bent-DEM pixel is identified to be a ground-clutter-contributing pixel if it is visible from the antenna focus. The visibility map is based on the output of block 2 using a simplified procedure. It is able to determine whether the pixels are visible from the radar site with sufficient accuracy in a time shorter than the one needed by similar routines available in GIS software by almost two orders of magnitude. Such a result is particularly useful to run GECS in reasonable time, even on a PC. In our simplified approach, the decision-making test concerning the visibility of the current pixel compares the ''visibility angle'' of the ''previous pixel'' with the radar-target zenith angle of the ''new pixel.'' If this last angle is less than the previous pixel visibility angle, the pixel is called visible; then its radar-target zenith angle value becomes its visibility angle and the pixel value is set to 1 in the visibility map. Otherwise, the previous pixel visibility angle is assigned to the visibility angle of the pixel at hand, and the value 0 is attributed in the visibility map; then the procedure goes on. The visibility angle of the pixel nearest to the radar is coincident with its radar-target zenith angle. This procedure allows the implemented algorithm to test the visibility condition of a given pixel simply by comparing the actual with the previous pixel visibility angle (without the need to examine all the pixels along the line between the radar and the actual pixel, thus speeding up the execution time). Because of raster structure (pixel quantization), pixel centers are usually not on the line of sight between the radar and the pixel of interest. There are several ways of taking into account neighboring pixels. In the present approach, only two neighboring pixels have been considered and a weighted average has been computed; the result is defined as the visibility angle of the previous pixel. We found this approximation to be reasonable for identifying ground clutter, especially considering the primary goals of simplicity and short simulation time.

Block 7 calculates the minimum height of a target for it to be optically seen by the radar (half of the beam can be blocked).

Once the raster maps of the radar-target zenith angle

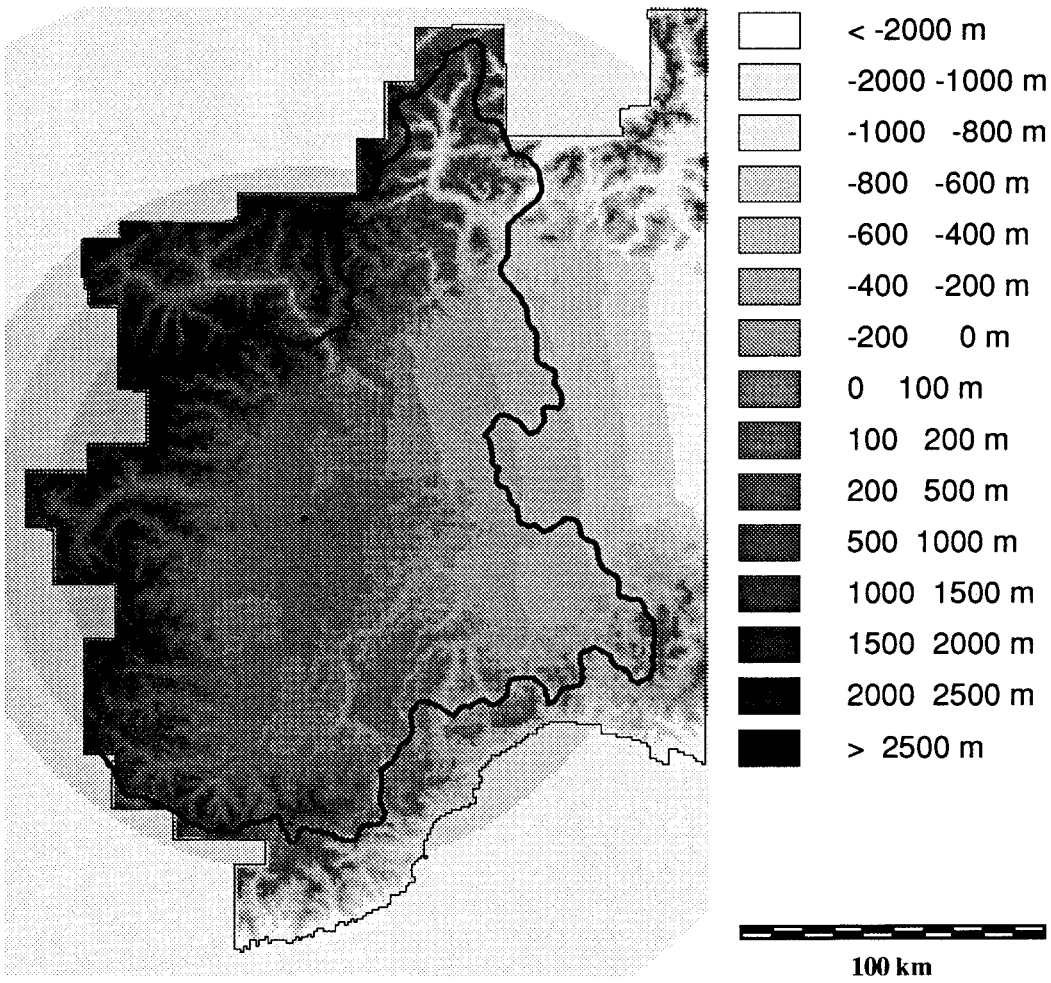

FIG. 3. Bent and resampled DEM registered on the radar Cartesian map (known atmospheric refractivity profile: $R_{eq}/R_{earth} = 1.34$).

(Φ_t), azimuth angle (Θ_t), local slope (β), and orientation (α) have been generated, the local angle of incidence θ_{inc} for each visible pixel is evaluated as $\theta_{inc} = \arccos(-\mathbf{r} \cdot \mathbf{n})$, where $\mathbf{r}$ is the unit vector along the line of sight linking the antenna focus to the ground clutter pixel and $\mathbf{n}$ is the unit vector normal to the slope surface (block 8).

Radar ground return is described in terms of σ^0, the scattering cross section per unit area (block 9). Even though information about a land-scattering cross section per unit area is now available (see, for instance, the compendia by Ulaby and Dobson 1989; Colwell et al. 1983; Ulaby et al. 1982), the literature on land clutter and related theoretical analysis is far from complete owing to the great number of variables characterizing land surfaces. For horizontal polarization (the only polarization state dealt with in the present paper), there are only very few σ^0 measuring campaigns concerned with a grazing angle less than 10° (Katz and Spetner 1960; Krason and Randing 1966). Land-based radar clutter originates mainly at such grazing incidence; in fact, in the present work, 94% of the angles of incidence are larger than 80°. A comprehensive model, the so-called linear model, for the average value of σ^0 expressed in decibels, $\overline{\sigma}^0_{dB}$, is presented by Moore (Skolnik 1990, chapter 12). Such a model was fitted to $\overline{\sigma}^0_{dB}$ versus the angle of incidence for the 6–17-GHz range. The author recommends using the derived parameters in the so-called plateau region, that is, for angles of incidence up to approximately 70°. Recently, Delrieu et al. (1995) performed measurements of $\overline{\sigma}^0_{dB}$ in the X band (horizontal polarization) with angles of incidence mainly between 71°–83°, extending above the linear model with different parameters in this ''near-grazing'' or ''shadow'' region. Furthermore, also for X band (horizontal polarization), Katz and Spetner (1960) have shown that at angles of incidence of approximately 87°–88°, $\overline{\sigma}^0_{dB}$ presents a minimum and then slightly increases again. Due to the paucity of experimental data in the simulation described in section 3, $\overline{\sigma}^0$ has simply been represented with the functional form $\gamma \cos\theta_{inc}$ (see Fig. 2). However, the presence of many pixels close to grazing angles suggests the need to adopt a more refined model in the

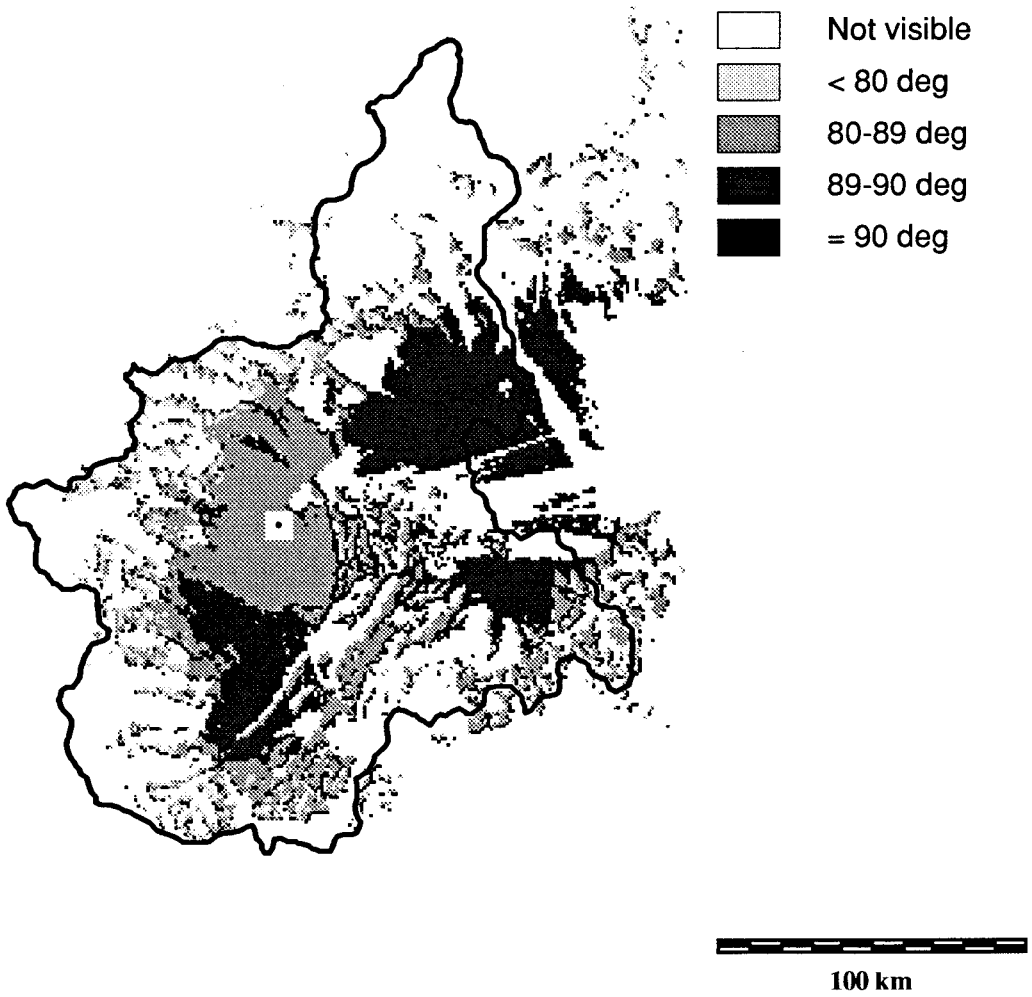

FIG. 4. Angles of incidence map ($R_{eq}/R_{earth} = 1.34$). The white 10 km × 10 km square area centered around the radar site (black circle) is the zone where no data are acquired.

future. For instance, taking into account all of the preceding considerations, a functional form for $\overline{\sigma}^0$ at large angles of incidence may be the following:

$$\overline{\sigma}^0(\theta_{\text{inc}}) = \begin{cases} \gamma \cos\theta_{\text{inc}}, \\ \quad \text{if } \theta_{\text{inc}} < \theta_1, \\ \gamma \cos\theta_{\text{inc}} \left[\dfrac{\pi/2 - \theta_{\text{inc}}}{\pi/2 - \theta_1}\right]^k, \\ \quad \text{if } \theta_1 < \theta_{\text{inc}} < \theta_2, \\ \gamma \cos\theta_2 \left[\dfrac{\pi/2 - \theta_2}{\pi/2 - \theta_1}\right]^k, \\ \quad \text{if } \theta_2 < \theta_{\text{inc}} < \theta_3, \\ \gamma \cos\theta_2 \left[\dfrac{\pi/2 - \theta_2}{\pi/2 - \theta_1}\right]^k \exp\left(\dfrac{\theta_{\text{inc}} - \theta_3}{b}\right), \\ \quad \text{if } \theta_3 \le \theta_{\text{inc}} \le 90°, \end{cases} \tag{1}$$

where the first angular region ($\theta_{\text{inc}} < \theta_1$) corresponds to the plateau region and the second one corresponds to the near-grazing or shadow region. Figure 2 shows $\overline{\sigma}^0$ versus θ_{inc} (1), having chosen $\gamma = 0.1$, $k = 1$, $\theta_1 = 80°$, $\theta_2 = 87°$, $\theta_3 = 88°$, and $b = 2.75°$, together with literature results cited before (the curves refer to horizontal polarization; for vertical polarization they might be quite different). Owing to the lack of experimental data at such grazing angles, the values for the constants in (1) are only exemplary. Figure 2 shows considerable variation of $\overline{\sigma}^0$ for a given angle of incidence. This is caused by the large variability of targets in the radar beam.

It is even more difficult (Nathanson 1969; Long 1975) to give an adequate statistical distribution of the stochastic variation of σ^0 for the following reasons: returns from a given area cannot easily be related to the land type because land surfaces are seldom homogeneous; the moisture content of the soil or the presence of snowcover can alter the scattering cross section per unit area;

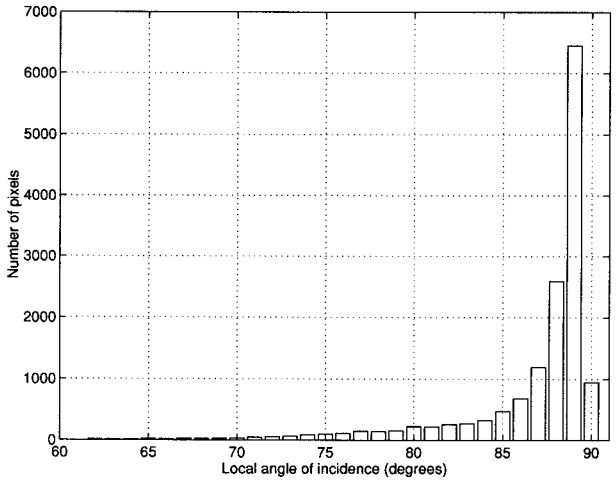

FIG. 5. Histogram of the angles of incidence map represented in Fig. 4 with 1 ° resolution (mean value = 87°, median value = 89°, standard deviation = 3.7°, and interquartile range = 2° centered at 88°).

also, mean and median values of σ^0 may be different depending on the history of measurements—whether ground-based or airborne measurements are considered (usually, ground-based radars perform time averages of a given clutter cell, while airborne radars perform spatial averages). Furthermore, at low grazing angles land backscatter is not usually Rayleigh distributed because of partial shadowing effects from terrain irregularities, buildings, trees, etc. The present version of GECS does not simulate any statistical fluctuations.

The first step consists in calculating (2), the received power P_t from each individual pixel of the DEM [having Cartesian coordinates (x_t, y_t), spherical coordinates (r_t, Θ_t, Φ_t), effective area $\Delta A_{t,\text{eff}} = \Delta x \cdot \Delta y/\cos\beta$]:

$$P_r(x_t, y_t) = \underbrace{\frac{P\lambda^2}{(4\pi)^3} G_0^2 \frac{1}{r_t^4}}_{C_r} f^4(\theta_t, \phi_t)\sigma^0(\theta_{\text{inc}})\Delta A_{t,\text{eff}}, \quad (2)$$

where P is the transmitted power, λ is the wavelength, G_0 is the antenna power gain along the beam axis, $f^4(\theta_t, \phi_t)$ is the square of the normalized power gain pattern in the target direction, and θ_t and ϕ_t are the angular coordinates with respect to the radar beam axis having angular coordinates (Θ, Φ).

If a region illuminated by a radar contains n DEM pixels, the received powers may be added:

$$\overline{P} = C_r \sum_{j=1}^{n} \frac{f^4(\theta_j, \phi_j)}{r_j^4} \sigma_j^0(\theta_{\text{inc}})\Delta A_{j,\text{eff}}. \quad (3)$$

The bar over P indicates the average value of the returned power. Size and shape of the illuminated region depend on angular and range weighting functions (Doviak and Zrnic 1993). Details on the intersection of the radar resolution volume and an elemental planar surface have been obtained and exhaustively described by Delrieu et al. (1995); in the present example, the ''approximate'' illuminated area is determined by means of the following simplified range and angular weighting functions:

- the range resolution is given by four samples added in range to obtain a polar cell; and
- a symmetric paraboloid antenna is considered. Hence, the angular one-way antenna power gain pattern $G(\theta_t, \phi_t)$ simplifies to $G(\psi) = G_0 f^2(\psi)$, where the square of the normalized power gain pattern $f^2(\psi)$ is user definable. Furthermore, it has been assumed that negligible contributions come from pixels with azimuthal angular distance greater than a threshold value ψ_{Max}.

3. Preliminary validation of the model

For the validation of the model, the results for a known atmospheric refractivity profile are compared with clear-sky data simultaneously acquired by the Regione Piemonte weather radar. For comparison purposes, the radar is following its normal data acquisition protocol with its clutter rejection algorithm disabled.

The main features of the radar system are listed in Table 1. The raw radar data are averaged over four range bins of 250 m each (each range bin is in turn the average of 15 gates) and resampled on a regular Cartesian kilometric grid. The available data consist of a projection of maximum reflectivity detected by the radar over the entire columnar volume above each pixel. In the near range (ranges lower than 20 km), real data values acquired at 0° elevation angle are completely ignored because, in the normal operational mode for weather echo acquisition, such values are always contaminated by ground clutter. This elimination causes a circular feature, clearly shown in both the real and the simulated maps. The volumetric scanning protocol requires 5 min to go through 14 progressive elevations; it starts at 0° elevation angle and ends at 19.5° with constant increases of 1.5° at each turn. GECS simulates this volumetric scanning of the radar antenna.

The area concerned, located in the northwest part of Italy, is a flat and hilly land surrounded by high mountains (Ligurian Apennines and the Alps) except for the eastern side, where the Po River valley gently slopes down to the Adriatic Sea. The radar is located on the top of the Bric della Croce peak at 710 m above mean sea level (MSL) and is surrounded mainly by flatlands approximately 200–300 m MSL. Consequently, radar echoes are strongly contaminated by ground clutter (especially next to the radar and eastward to the Po River valley). In the present example, the DEM used is a 30 s × 30 s (approximately 928 m × 656 m DEM, available in the TerrainBase CD-ROM release 1.0 developed by Row et al. 1995). The project was conducted by the National Geophysical Data Centers to develop a research-quality worldwide collection of digital elevation

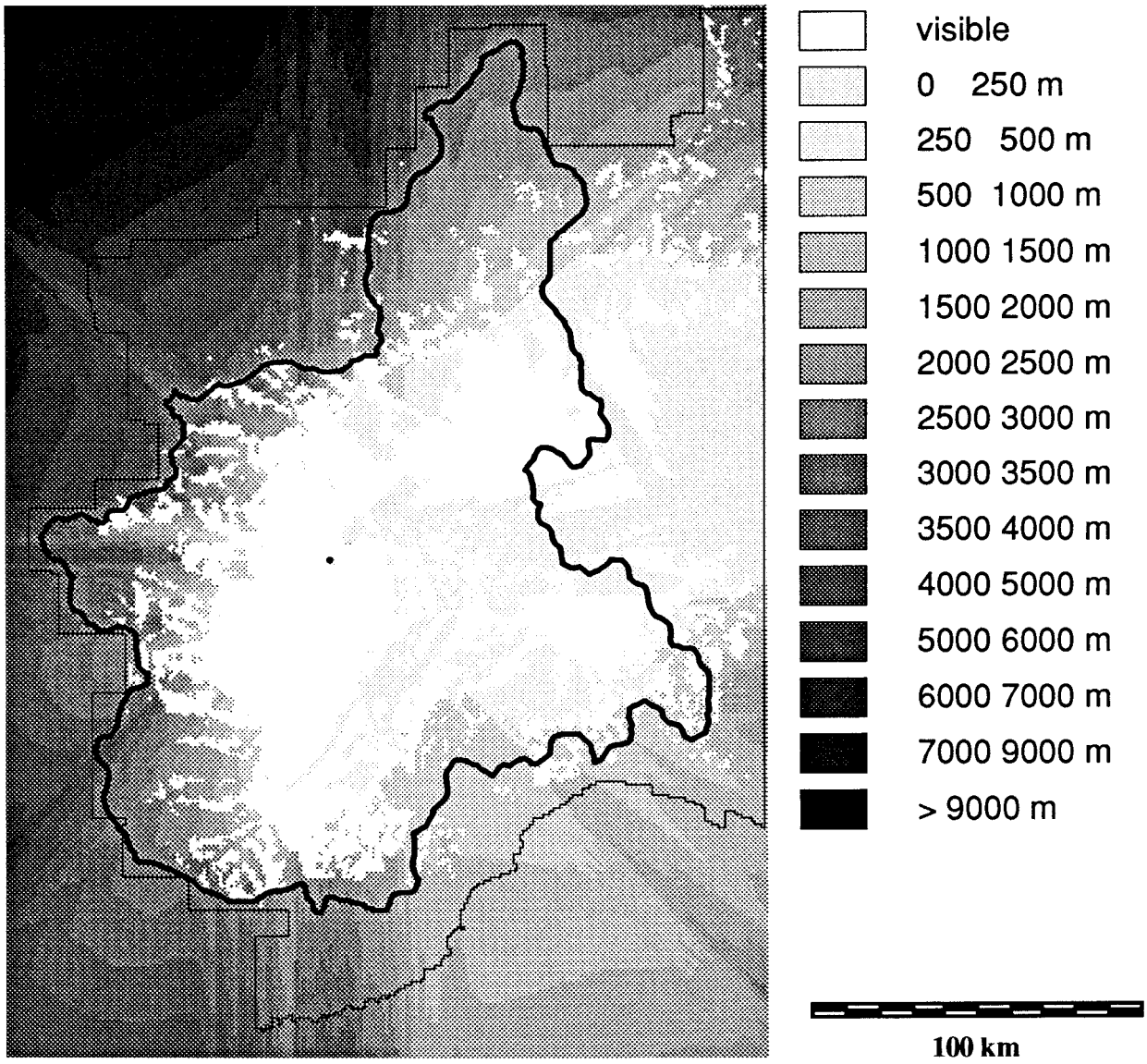

FIG. 6. Minimum height (MSL) that a meteorological target must reach to be optically seen from the radar site ($R_{eq}/R_{earth} = 1.34$).

models. It seemed advantageous for simulation speed to deal directly with resampled and registered DEM pixels having the same spatial resolution of the radar Cartesian maps (1 km $\times$ 1 km). Even such coarse resampled DEM gives, at large distances, multiple ground pixels for each radar resolution cell. Figure 3 represents the bent and resampled DEM registered on the radar Cartesian map (340 rows $\times$ 340 columns). Among the 115 600 pixels only 51 000 contain real height value, precisely those corresponding to the Italian territory and Ligurian Sea (outside Italy, only data with a much coarser resolution were available). However, due to shielding by the Alps, no significant ground clutter is found outside this region.

Figure 4 shows a map of angles of incidence for pixels visible from the radar site (13 936 out of 51 000 pixels, corresponding to 27.3%) for a known atmospheric refractivity profile (1100 UTC 6 December 1994); simultaneous radio soundings in the Milano Linate airport (approximately 110 km east of the radar) showed a quasi-constant value of refractivity gradient in the first kilometer of the atmosphere. This corresponds to the equivalent earth radius used in the simulation stage ($R_{eq}/R_{earth} = 1.34$). The histogram of this map (Fig. 5) shows that no pixel presents an angle of incidence lower than 62° and that for more than 94% of the pixels, the scattering from terrain takes place at angles greater than 80°. The distribution is unimodal and rather highly skewed.

Figure 6 shows the minimum height (MSL) that a target must reach to be optically seen from the radar ($R_{eq}/R_{earth} = 1.34$). This image allows to estimate errors

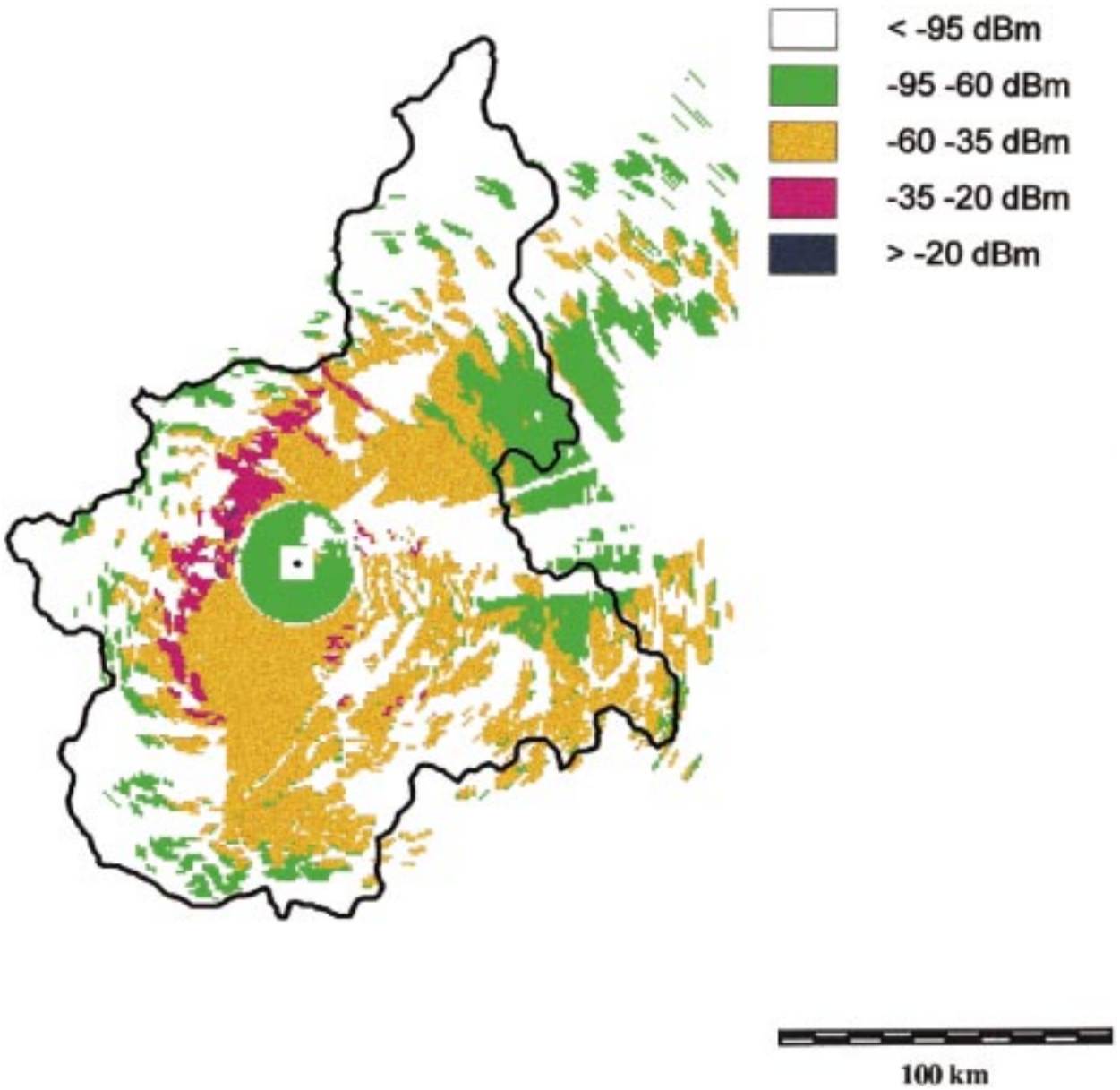

FIG. 7. Simulated ground clutter in clear-sky, dry weather condition ($R_{eq}/R_{earth} = 1.34$).

caused by a decrease of reflectivity with height. Obviously, the height difference between the ground and the minimum ''radar visibility altitude'' is an important indicator of the achievable accuracy in estimating precipitation rate at ground level.

A display of the simulated ground clutter returns is presented in Fig. 7. In any range bin, the effects of lateral pixels have been considered assuming a threshold value ψ_{Max} equal to 3°. By visual comparison, the similarity is evident between the simulation (Fig. 7) and the power measured by the radar (Fig. 8). The overall matching between the two ground clutter patterns of Figs. 7 and 8, as well as the shadowed area locations, is good. [It must be noted that ground clutter structures radially departing from the radar in the northeast and southwest directions of the real map (Fig. 8) are due to shadowing effects by nearby towers not reflected by the DEM.] Of course, the measured pattern shows more small-scale variations in clutter intensity (speckle noise in measurements that can be reduced by averaging several maps). Such small-scale variations are also caused by the presence of urban areas not inserted in the $\overline{\sigma}^0$ scattering model. The difficulty in implementing a more realistic surface scattering model is not only caused by the lack of experimental values of $\overline{\sigma}^0$ at near-grazing angles but also by the absence of a land use–land cover map detailed enough for the calculation. Furthermore, a DEM with a higher spatial

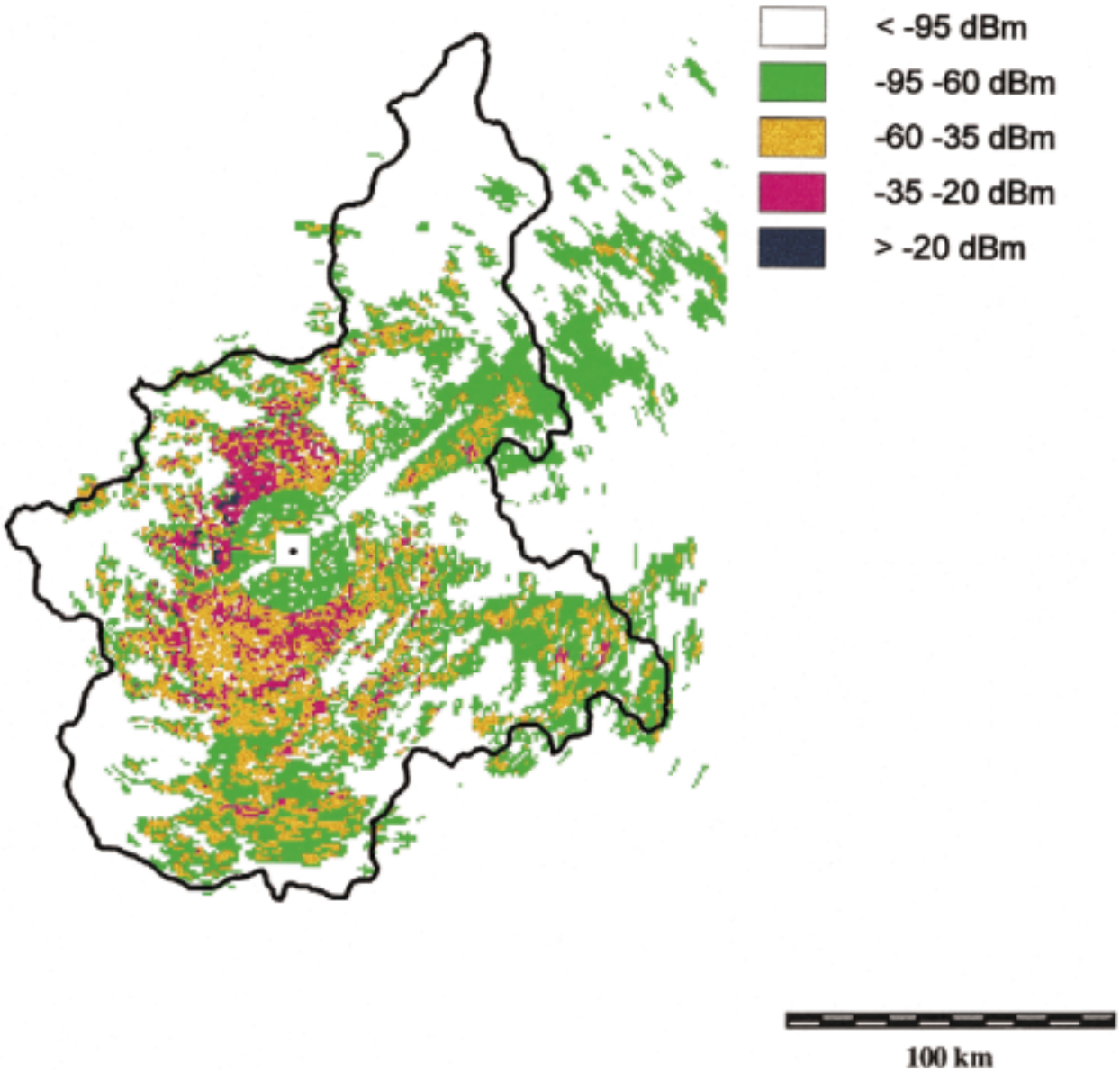

FIG. 8. Ground clutter power measured by the radar situation at 1100 UTC 6 December 1994 (clear-sky, dry weather condition and quasi-constant value of atmospheric refractivity profile: $R_{eq}/R_{earth} = 1.34$).

resolution should be adopted (especially in the mountainous areas).

4. Conclusions and potential

A software tool for the characterization of the orographic environment of operational meteorological radars has been presented. Important radar meteorology–related activities, such as radar siting and estimate of precipitation rate at ground level, could benefit from it. On the one hand, maps of ground clutter areal distribution can be used for the preliminary characterization of a radar site; on the other hand, information concerning the minimum height at which a given volumetric pixel of the atmosphere is optically seen by the radar beam is very useful as input to correction procedures based on measured vertical profiles of precipitation rate.

The implemented software can be also useful for the following activities:

- optimum choice of the minimum elevation angle in the antenna scan program;
- detection of possible misalignments in azimuth (through the analysis and comparison of simulated and measured ground target with operative scanning-program procedures); and
- analysis for terrain-dependent line of sight for radio links.

Furthermore, the software could be used to improve the understanding of backscatter from terrain at low grazing angles (which still creates severe problems in the detection of small, low-altitude aircraft; surface targets; and nonradially moving hydrometeors). Of course, a high-resolution DEM and a reliable land use–land cover map should be available. GECS can estimate in advance the attributes of any specific radar site and radar system. The raster-based approach used in implementing the code makes it compatible with the desired spatial resolution because the CPU time is inversely proportional to the desired spatial resolution.

Simplicity and short simulation times have been pursued as primary goals during the planning and implementation phases of the code. The result is a standard ANSI FORTRAN software that is portable, easy to use, and runs on IBM-compatible PC. In its simplest version, the model needs only a raster Digital Elevation Model, the radar parameters, and an estimate of the mean atmospheric refraction.

Acknowledgments. The comments made by the anonymous reviewers were very useful in making this paper more clear and more concise.

APPENDIX

List of Symbols

In order of appearance in the text.

β	Pixel slope
α	Pixel orientation
Φ_t, Θ_t	Radar-target angular coordinates (zenith and azimuth)
$\mathbf{n}$	Unit vector normal to the slope surface
$\mathbf{r}$	Unit vector along the antenna-pixel line of sight
θ_{inc}	Local angle of incidence
r_t	Radar-target distance
σ^0	Scattering cross section per unit area (or differential scattering cross section or backscattering coefficient)
$\overline{\sigma}^0$	Average scattering cross section per unit area
γ, k, b	Parameters for $\overline{\sigma}^0$
θ_1, θ_2, θ_3	Limit of angular regions of incidence
$P_r(x_t, y_t)$	Received power by target pixel
x_t, y_t	Target pixel Cartesian coordinates
P	Transmitted power
λ	Wavelength
G_0	Antenna power gain along the beam axis
$f^2(\theta_t, \phi_t)$	Normalized power gain in the target direction
Φ, Θ	Radar beam axis angular coordinates
ϕ_t, θ_t	Target angular coordinates taken with respect to the radar beam axis ($\phi_t = \Phi - \Phi_t$, $\theta_t = \Theta - \Theta_t$)
$A_{t,\text{eff}}$	Target pixel effective area
τ	Pulse duration
ψ	Angular distance from the radar beam axis
ψ_{Max}	Angular threshold for antenna gain
R_{eq}	Equivalent earth radius
R_{earth}	Earth radius

REFERENCES

Colwell, R. N., D. S. Simonett, J. E. Estes, F. T. Ulaby, and G. T. Thorley, 1983: *Manual of Remote Sensing.* 2d ed. Vols. 1 and 2. American Society of Photogrammetry, 2440 pp.

Delrieu, G., J. D. Creutin, and H. Andrieu, 1995: Simulation of radar mountain returns using a digitized terrain model. *J. Atmos. Oceanic Technol.,* **12,** 1038–1049.

Doviak, R. J., and D. S. Zrnic, 1985: Siting of Doppler weather radars to shield ground targets. *IEEE Trans. Antennas Propag.,* **33,** 685–689.

——, and ——, 1993: *Doppler Radar and Weather Observations.* 2d ed. Academic Press, 562 pp.

Eastman, J. R., 1990: IDRISI—A Grid-Based Geographic Analysis System. Version 4.1. Clark University.

Geotis, S. G., and W. M. Silver, 1976: An evaluation of techniques for automatic ground-echo rejection. Preprints, *17th Conf. on Radar Meteorology,* Seattle, WA, Amer. Meteor. Soc., 448–452.

Joss, J., and H. Wessels, 1990: Ground clutter suppression for weather radar data. COST 73/WD/130, 6 pp. [Available from Office for Official Publications of the European Communities, L-2985 Luxembourg.]

——, and R. Lee, 1995: The application of radar–gauge comparisons to operational precipitation profile corrections. *J. Appl. Meteor.,* **34,** 2612–2630.

——, G. Galli, A. Pittini, G. Della Bruna, and R. Lee, 1995: Seven years of (dis)agreement between radar, rain gauges and river flow: Possible improvements? Preprints, *27th Int. Conf. on Radar Meteorology,* Vail, CO, Amer. Meteor. Soc., 29–30.

Katz, I., and L. M. Spetner, 1960: Polarization and depression angle dependence of radar terrain return. *J. Res. Nat. Bur. Stand.,* **64D,** 483–486.

Krason, H., and G. Randing, 1966: Terrain backscattering characteristics at low grazing angles for X- and S-band. *Proc. IEEE,* **54,** 1964–1965.

Lee, R., G. Della Bruna, and J. Joss, 1995: Intensity of ground clutter and of echoes of anomalous propagation and its elimination. Preprints, *27th Int. Conf. on Radar Meteorology,* Vail, CO, Amer. Meteor. Soc., 651–652.

Long, M. W., 1975: *Radar Reflectivity of Land and Sea.* Lexington Books, 366 pp.

Nathanson, F. E., 1969: *Radar Design Principles.* McGraw-Hill, 626 pp.

Row, L. W., D. A. Hastings, and P. K. Dunbar, 1995: Documentation manual for TerrainBase—Worldwide Digital Terrain Data, CD-ROM, Release 1.0, NGDC Key to Geophysical Records Documentation 30, National Geophysical Data Center, National Oceanic and Atmospheric Administration, Boulder, CO, 169 pp. [Available from NOAA/NGDC, 325 Broadway, Boulder, CO 80303-3328.]

Skolnik, M. I., 1990: *Radar Handbook.* 2d ed. McGraw Hill, 1037 pp.

Smith, P. L., 1972: Siting considerations for weather radars. Preprints, *15th Conf. on Radar Meteorology,* Champaign–Urbana, IL, Amer. Meteor. Soc., 99–100.

Ulaby, F. T., and M. C. Dobson, 1989: *Handbook of Radar Scattering Statistics for Terrain.* Artech House, 357 pp.

——, R. K. Moore, and A. K. Fung, 1982: *Microwave Remote Sensing: Active and Passive.* Vol. 2. Addison-Wesley, 2162 pp.